Low-force compressive and tensile actuation for elastocaloric heat pumps

Agata Czernuszewicz[a*], Lucas Griffith[a], Julie Slaughter[a], Vitalij Pecharsky[a,b]

[a] *Ames Laboratory, U.S. Department of Energy, Iowa State University, Ames, IA 50011, USA*

[b] *Department of Materials Science and Engineering, Iowa State University, Ames, IA 50011, USA*

HIGHLIGHTS

- Elastocaloric material-polymer composite structures can be actuated by bending.
- Active materials are entirely under either tension or compression in the composite.
- Forces required to actuate NiTi prototype are reduced by more than 50%.

ABSTRACT

The elastocaloric effect underpins a promising solid-state heat pumping technology that, when adopted for commercial and residential applications, can revolutionize the cooling and heating industry due to low environmental impact and substantial energy savings. Known operational demonstration devices based on the elastocaloric effect suffer from low endurance of materials and, in most experimental systems, from large footprints due to bulky actuators required to provide sufficient forces and displacements. We demonstrate a new approach which has the potential to enable a more effective exploitation of the elastocaloric effect by reducing the forces required for actuation. Thin strips of NiTi were incorporated into composite structures with base polymer, such that bending the structures results in either exclusively compression or exclusively tension applied to the elastocaloric strips. The structures allow compression of thin elastocaloric strips without buckling, realize more than 50% reduction in required forces for a given strain compared with axial loading, and open up a wide range of possibilities for compact, efficient elastocaloric devices.

Keywords: Elastocaloric effect; NiTi; Solid-state refrigeration; Strain gauges; Superelasticity

Nomenclature

B	width of the beam (m)
c	distance between neutral surface and outer fiber of the beam (m)
c_p	specific heat at constant pressure (J kg^{-1} K^{-1})
F	force (N)

[*] Corresponding author.
E-mail address: acz@ameslab.gov (A. Czernuszewicz).

H	height of the beam (m)
I_y	moment of inertia (N m)
J	heat flux (W m^{-2})
k	thermal conductivity (W m^{-1} K^{-1})
L	length of the beam (m)
M_g	bending moment (N m)
Q	heat (J)
t	time (s)
T	temperature (K)
Δt	time change (s)
ΔT	temperature change (K)
V	volume (m^3)
y	distance from the neutral axis (m)
ε	strain (%)
σ	stress (MPa)
ρ	density (kg m^{-3})
PEEK	Polyether Ether Ketone

1 Introduction

Vapor-compression technology consumes *ca* 6 EJ of the 37 EJ of primary energy used annually in the United States, to dehumidify, cool and heat space, and chill water [1]. Fractions of energy consumed for similar uses in the developed countries are comparable to the U.S., and they are rapidly growing in the developing world. Caloric heat pumping promises to become an energy efficient and environmentally benign alternative to vapor-compression methods in common use today. In addition to potential energy savings as high as 25 to 30% [2], a transition to caloric heat pumping technologies also replaces the potent greenhouse gases currently used as refrigerants with zero global-warming-potential caloric solids. The most mature caloric technology is based on the magnetocaloric effect [3], which is a reversible thermal response of a solid magnetic material subjected to adiabatic changes of an external magnetic field. Laboratory-scale refrigeration devices based on the magnetocaloric effect already demonstrate temperature spans and cooling powers sufficient for some applications [2,4], however, the high cost of generating magnetic field changes on the order of 1.1 – 1.5 T impedes the introduction of the technology to the market. Another phenomenon that attracts increasing attention because of its potential for high energy conversion efficiency, is the elastocaloric effect, where reversible adiabatic temperature changes in certain superelastic materials can be

generated by stress. The key advantages of elastocaloric cooling over magnetocaloric are that stress-generating components may, in principle, be realized at low cost, and the maximum achievable stresses are much less limited than the maximum magnetic fields available from either permanent or superconducting magnets.

Several laboratory-scale demonstration cooling systems employing the elastocaloric effect have been reported in the literature [5], demonstrating coefficients of performance as high as 7 [6], which is in line with the material-based coefficient of performance reaching 11.8 (83.7% of Carnot) theoretically predicted for NiTi (Nitinol) [7]. Most of the known systems are bulky because hydraulic load frames are used to generate the high force/displacement required to maximize temperature changes [6,8,9]. Moreover, the working elastocaloric material (NiTi), is mainly actuated by tensile stress which, though easy to apply, greatly reduces life-span of materials due to fatigue [10,11]. More recently, methods of harnessing the elastocaloric effect potentially applicable to variable-scale cooling systems have been reported. One such approach uses a magnetostrictive material where stress is generated by a low magnetic field (0.16 T), to cyclically compress a 2 x 1 x 2 mm^3 $Cu_{72}Al_{17}Mn_{11}$ sample [12]. Though more elegant than a hydraulic load frame, the high cost of advanced magnetostrictive materials and unfavorable length ratios of the magnetostrictive and elastocaloric components (proportional to strain, on the order of 10^{-2}, required to actuate the latter, but inversely proportional to magnetostriction, on the order of 10^{-3}, of the former) are major weaknesses of this strategy. Elastocaloric materials can be also actuated by torsion. Wang *et al.* [13] describe a method of cooling by winding wires which results in specific cooling energy of 7.9 J g^{-1} and temperature change up to 20.8 K for NiTi. The nonuniform temperature change, however, demonstrates the inhomogeneous stress distribution in the twisted material.

Another method of inducing the elastocaloric effect is bending the material [14–17]. Sharar *et al.* [14] demonstrate a six-fold reduction of the force required to generate a given strain on the surface when bending 1 mm NiTi wire as compared to direct tensile loading. Bending, however, results in a distribution of stress and strain (from compression on the inside of the bend radius to tension on the outside), which makes parts of the active material under tension susceptible to fatigue and reduces the temperature response; in this case from 16 K in tension to 9 K during bending. Ossmer *et al.* [15] and Bruederlin *et al.* [16] report a miniature-scale heat pump that operates by stretching a 30 µm thick $Ti_{49.1}Ni_{50.5}Fe_{0.4}$ foil over cleverly shaped heat exchangers. The system consists of an elastocaloric bridge attached to a movable frame, and solid heat exchangers. The device uses the adiabatic temperature change of the material directly, which generally results in a simpler device, but limits the temperature span between the hot and cold sides to less than the generated adiabatic temperature change. A model of another miniature elastocaloric system to provide temperature span larger than the adiabatic temperature change of the material was described in [17]. A

cantilever-based device with patches of piezoelectric $0.50Ba(Zr_{0.2}Ti_{0.8})O_3-0.50(Ba_{0.7}Ca_{0.3})TiO_3$ was actuated by vibrations. According to the model, a single cantilever could generate 0.2 K temperature change at 324 K, while 10 cascaded elements could create a temperature difference of about 2 K in 10 s.

Though elastocaloric cooling remains promising, there are many barriers that must be overcome before this technology can be employed practically. As mentioned before, one of the major hindrances is the high forces necessary to obtain sufficient adiabatic temperature changes, which translates into bulky and expensive actuators. Another hurdle is short fatigue life of materials subjected to tension. Tensile loading allows for use of samples with very high length to thickness ratio (e.g. strips, plates, foils, ribbons) which is highly beneficial for heat transfer; however, cracks open in working elements under the tensile stress, reducing their lifetime much below the $\sim 10^{8\text{-}9}$ cycles required for a typical appliance. Materials subjected to compression loading can endure many more cycles, but their shapes are limited to short lengths with large cross-sectional areas to avoid buckling which strongly limits heat transfer and reduces performance of a compression-based device. While tubes [9] tolerate compression and provide reasonably good heat transfer, they are also much more expensive than wires or thin plates. Compression often also requires higher stresses than tension to obtain the same strain [18] and, therefore, temperature change.

In this work we describe a novel low-force method of activating thin strips of elastocaloric material in *either tension or compression* for applications in future efficient solid-state heat pumping systems. Strips of NiTi were incorporated into structures that reduce the actuating forces. Fabricated beams consisted of patches of active material and a plastic base material with low thermal conductivity to reduce parasitic heat losses. In tensile configuration, large strains and stresses were achieved with less than ½ the force of direct tension. In a compression configuration, a NiTi strip was bonded directly to a plastic beam; when this beam was tested in a four-point bend setup, the entire strip was in compression. This configuration also used approximately ½ of the force as with direct actuation, and, more importantly, it allowed the entire sample to be in compression without buckling. The proposed concept paves the way to the new, potentially exciting area of compact and efficient elastocaloric systems.

2 Materials

A Ni-Ti superelastic alloy containing 50.6 to 51.0 at.% Nickel (henceforth NiTi) with the quoted austenite finish temperature around 290 K was purchased from Confluent. The material was received in strips 0.2 mm thick by 4 mm wide and cut to 90 mm length. To increase fatigue life in tension, the edges of NiTi strips were surface treated by mechanical polishing. Differential scanning calorimetry traces of a sample extracted from a strip trained in tension are shown in Supplementary figure 1. High-strength Polyether ether ketone (PEEK) was used as a beam base material.

3 Methodology

3.1 Concept

The idea of reducing force required to axially actuate the elastocaloric material is based on a bending beam concept. Applying the force, F, axially gives a uniform stress, σ_{axial}, over the entire length of the beam:

$$\sigma_{axial} = \frac{F}{BH}, \tag{1}$$

where B, H – width and height of the beam, respectively.

A straight rectangular beam subjected to forces transverse to its axis deflects. The bending moment, M_g, causes tension on one side of the beam and compression on the other. The neutral surface is a curved surface at distance, c, from the outer fiber of the beam, on which no change in length occurs, hence there is no tension or compression. Strain and stress in a deflected beam are described [19] as:

$$\varepsilon_{bending} = -\frac{y}{c}\varepsilon_{max} = -\frac{y}{c}\varepsilon_c, \text{ and} \tag{2}$$

$$\sigma_{bending} = -\frac{y}{c}\sigma_{max} = -\frac{y}{c}\sigma_c, \tag{3}$$

where $\varepsilon_{bending}$ – strain in a bent beam, $\sigma_{bending}$ – stress in a bent beam, y – distance from the neutral axis, ε_c, ε_{max} - strain at the outer fiber of the beam which is distance c from the neutral axis, and σ_c, σ_{max} – stress at the outer fiber. According to equations (2) and (3) the outer fibers of the beam experience the largest strain and stress.

When the beam is subjected to four-point bending, the maximum stress and strain are constant over the section of the beam between loading points. If the loading span is ½ of the support span, stress in the beam between loading points can be calculated from [19]:

$$\sigma_{bending} = \frac{M_g y}{I_y} = \frac{F}{BH}\frac{3Ly}{2H^2} = \sigma_{axial}\frac{3Ly}{2H^2}, \tag{4}$$

where I_y – moment of inertia, L – length of the beam. Since the length is much larger than the height for a long, thin beam, bending stresses are much larger compared with axial loading for the same force as shown by the last term of (4).

In order to minimize the required force to achieve a given stress, NiTi strips and plastic beams were assembled as structures consisting of patches of NiTi attached to the outer surface of the beam and subjected to four-point bending. Structures are designed to assure the neutral surface is in the plastic beam, placing the elastocaloric material entirely in either tension or compression. Figure 1 shows a principle schematic of the proposed method for an elastocaloric material in compression.

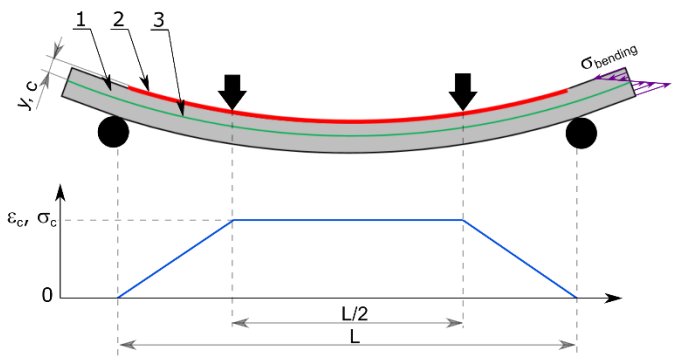

Figure 1 Principle schematic of the four-point bending method with elastocaloric material entirely in compression; 1 – base beam, 2 – elastocaloric material, 3 – neutral axis. Supporting pins are shown as circles and loading pins – as arrows.

3.2 Test system

A purpose-build test system enabled investigations of elastocaloric material performance under bending conditions. The main system components are: a linear actuator (1), load cell (2), and test fixtures (3, 4) as shown in Figure 2. The four-point bending fixtures have a fixed loading span of 60 mm, while the supporting span is 120 mm. The system is also equipped with tensile fixtures for direct tensile loading. The actuator from Progressive Automations has a 3-phase brushless DC motor drive with 100% duty cycle, allowing cyclic tests, a built-in 10 kΩ potentiometer for position sensing, a load capacity of 667 N, a 305 mm displacement, and a maximum speed of 15 mm s^{-1}. The 60001 Vishay Sensortronics S-type load cell has a 4448 N load range and can work in both compression and tension. The load cell combined error is ±1.33 N and non-repeatability is ±0.44 N. Variability during static measurements agrees well with the combined error, however variability during dynamic measurements increases with rising (un)loading rates to a maximum of ±10 N.

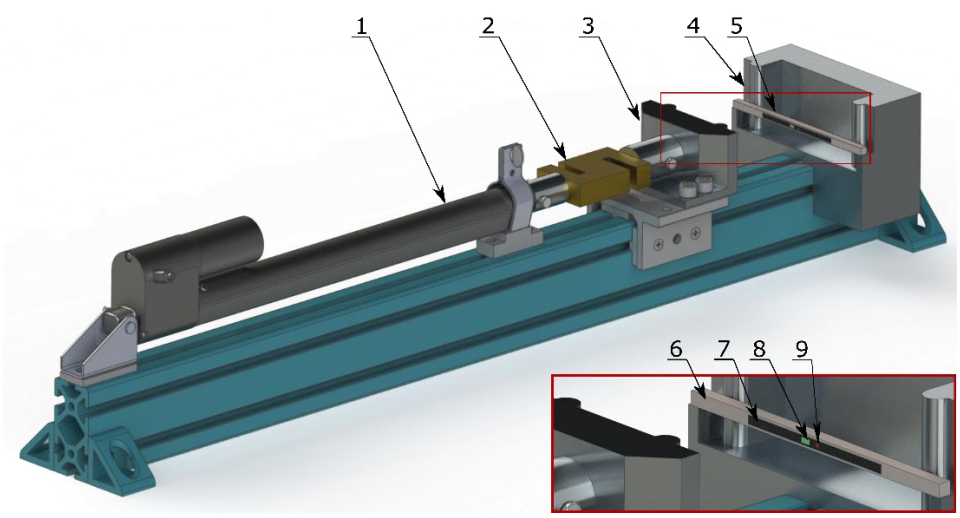

Figure 2 Solid model of experimental system: 1 – linear actuator, 2 – load cell, 3 – loading fixture for 4-point bending tests, 4 – supporting fixture for 4-point bending tests, 5 - sample, 6 – base beam, 7 – elastocaloric material, 8 – strain gauge, 9 - thermocouple

The elastocaloric system is controlled using Raspberry Pi 3 single board computer running Raspbian. It is equipped with modules for force, position, strain, speed, and temperature measurements. Temperature is monitored using T-type thermocouples with 0.08 mm wire diameter. Thermocouples are glued to the NiTi surface with high thermal conductivity epoxy to ensure a robust connection and fast response. Strain measurement provides precision of 14 με and accuracy of ±1.6%. Temperature measurement has accuracy of ±1 K with precision of 0.01 K. The accuracy of the position sensor is 0.05 mm with 0.01 mm precision and time delay of 0.1 s. Data logging is performed at all times during operation. Tests can be controlled with the force, position, or a combination of both. Thermocouple and strain gauge are attached to the top surface of the elastocaloric material and are located near the middle between the loading pins (strain gauge used to measure strain in tension was placed in a similar fashion but was attached to a passive material as will be discussed in the next section). Figure 2 also shows an enlarged view of a sample, including placement of the sensors. Characteristics of all components used to construct the experimental apparatus are provided in Supplementary table 1.

3.3 Strain measurement

Strain gauges are the natural choice for strain measurements owing to their ease of application and low cost, assuming they can be effectively bonded to the NiTi surface [20]. Uniaxial strain gauges SGT-1/350-TY11 from Omega and 1-LY11-0.6/120 from HBM of width 3.0 mm and 3.2 mm, respectively were bonded to the NiTi surface with adhesives Z 70 and X 60 from HBM. Sensors were arranged longitudinally and transversely which allows quarter or half-Wheatstone bridge circuit configuration (in half-bridge circuit configuration only the same type strain gauges were used). Initial validation of the system for axially loaded NiTi strip showed a significant difference between strain measured with the position sensor and strain measured by a strain gauge mounted longitudinally (Supplementary figure 2). The strain gauge response starts to saturate around 1%, conspicuously coinciding with the strain value where the phase transition initiates, indicating that the sensors may impede the martensitic transition in areas they cover. An IR camera (FLIR A8303sc) captured temperature changes in NiTi strips during tensile loading at a room temperature of 296.7 K both without the strain gauge attached and on the side opposite the mounted strain gauge as shown in Figure 3. A plot below the IR images illustrates temperature profiles along the lengths of both NiTi strips with each data point representing the average of 26 temperature readings (pixels) in the directions normal to the strip length.

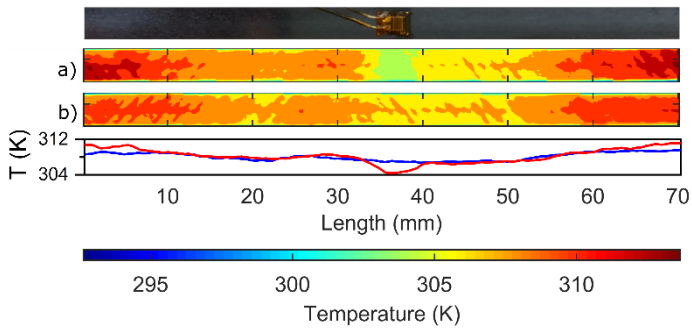

Figure 3 Optical image of the NiTi strip with the strain gauge attached (top), IR images of the strips under 4% tensile strain (a) with strain gauge (imaged on side opposite strain gauge) and (b) without strain gauge. Temperature profiles illustrated below the IR images in red and blue are, respectively, for the strips shown in (a) and (b).

IR image of the bare sample (Figure 3 (b)) shows a relatively uniform temperature distribution across the sample as indicated by the color scale largely in the yellow to red range (also see Supplementary figure 3). Minor non-uniformity in local temperature distribution seen as diagonal bands reflects locations of the Lüders-type bands where martensitic transition in NiTi is initiated by stress [10]. For the sample with the sensor mounted (Figure 3 (a)) a 4% strain change (as measured by the actuator position sensor) causes the change in temperature in the range from 7.65 to 17.25 K. Results show the lowest temperature changes where the strain gauge is affixed to the strip, as indicated by the green area. Though the temperature change is expected to be somewhat lower because of heating of the strain gauge due to heat conduction, the difference in the temperature change is too large to be explained by this effect alone. Moreover the changes in the temperature in areas away from the sensor are notably higher than ΔT in the bare sample. Since temperature change is proportional to strain, this confirms non-uniform strain distribution in the NiTi strip with the strain gauge attached. It is likely that if the sample width is much larger than the width of the strain gauge envelope, the influence of the sensor is lower making it possible to measure the strain in a loaded sample as was done in [20]. However, for narrow samples used in this work, it is difficult to find sensors small enough to directly measure strain of the NiTi strips in tension.

To correctly measure strain in NiTi strips in tension (clamped only on ends) strain gauges were bonded to a passive material mounted side by side with the NiTi strip to ensure identical strains. For this purpose, thin polycarbonate strips were chosen due to high yield point (above 2% strain). An additional benefit of using a passive material for measuring strain is that it thermally isolates the strain gauges, preventing any influence from elastocaloric effect on strain readings. The force required to stretch the polycarbonate strip itself was measured separately and subtracted from the NiTi measurements. Strains in excess of 2% were calculated from the position sensor for the directly loaded elastocaloric strips. In the bending mode strain was extrapolated from the superelastic slope and verified with the position sensor.

Samples where NiTi strips were directly bonded to a plastic beam and subjected to bending showed no saturation in strain, i.e. the measured strain increased linearly with the actuator position. In these samples, the stiffness of the plastic beam dominates over the stiffness of the NiTi and the sensor, and enables equal strain distribution along the loaded sample. Strain was measured directly on the NiTi strip in these samples.

4 Bending, tensile loading

4.1 Samples

Samples used in a bending mode, where elastocaloric material experiences only tensile stresses, consist of a strip of NiTi which is attached to a base beam (PEEK) with a large cutout as shown in Figure 4. The cutout reduces the beam stiffness allowing the elastocaloric material to dominate the overall stiffness. Moreover the slot ensures bilateral access to the active material which is favorable for heat transfer between the active material and heat transfer medium in future refrigerator configurations.

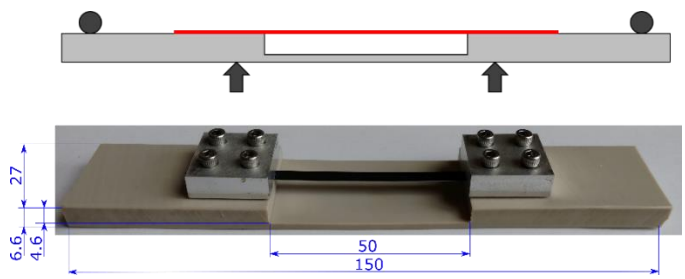

Figure 4 Sketch and photograph of the tension sample configuration with supporting pins shown by circles and loading pins shown by arrows

The PEEK beam used as a base material was 150 mm long, 27 mm wide, and 6.6 mm thick with a slot of 50 x 27 x 4.6 mm. NiTi strips were clamped to the beam on the side with the cutout. This beam structure ensures the 50 mm of NiTi strip above the slot is entirely in tension. Finite element modeling (Supplementary figure 4) demonstrates that the stress and strain distribution in that part of the strip is nearly homogenous (2% variation of strain over its thickness), and the neutral surface is located in the plastic beam.

4.2 Results and discussion

Before testing, NiTi materials were trained to stabilize their behaviors [10]. The NiTi strips were subjected to 150 loading/unloading cycles between 0 and 500 N (which corresponds to 625 MPa) using a strain rate of 0.05 s^{-1} at room temperature. The critical stress of the superelastic transition decreased from 480 MPa to 340 MPa after the training.

The elastocaloric effect in the trained samples was first evaluated in direct tension. Figure 5 shows measurements of temperature changes in axially loaded samples for strains from 0.5% to 6% with a preload

of 5 MPa, and strain rate of 0.05 s^{-1}. Because of the time delay of the potentiometer used to evaluate the strain above 2%, the force-strain curves in Figure 5 (c), and also in panel (c) of Figure 6, are plotted only up to 2% strain.

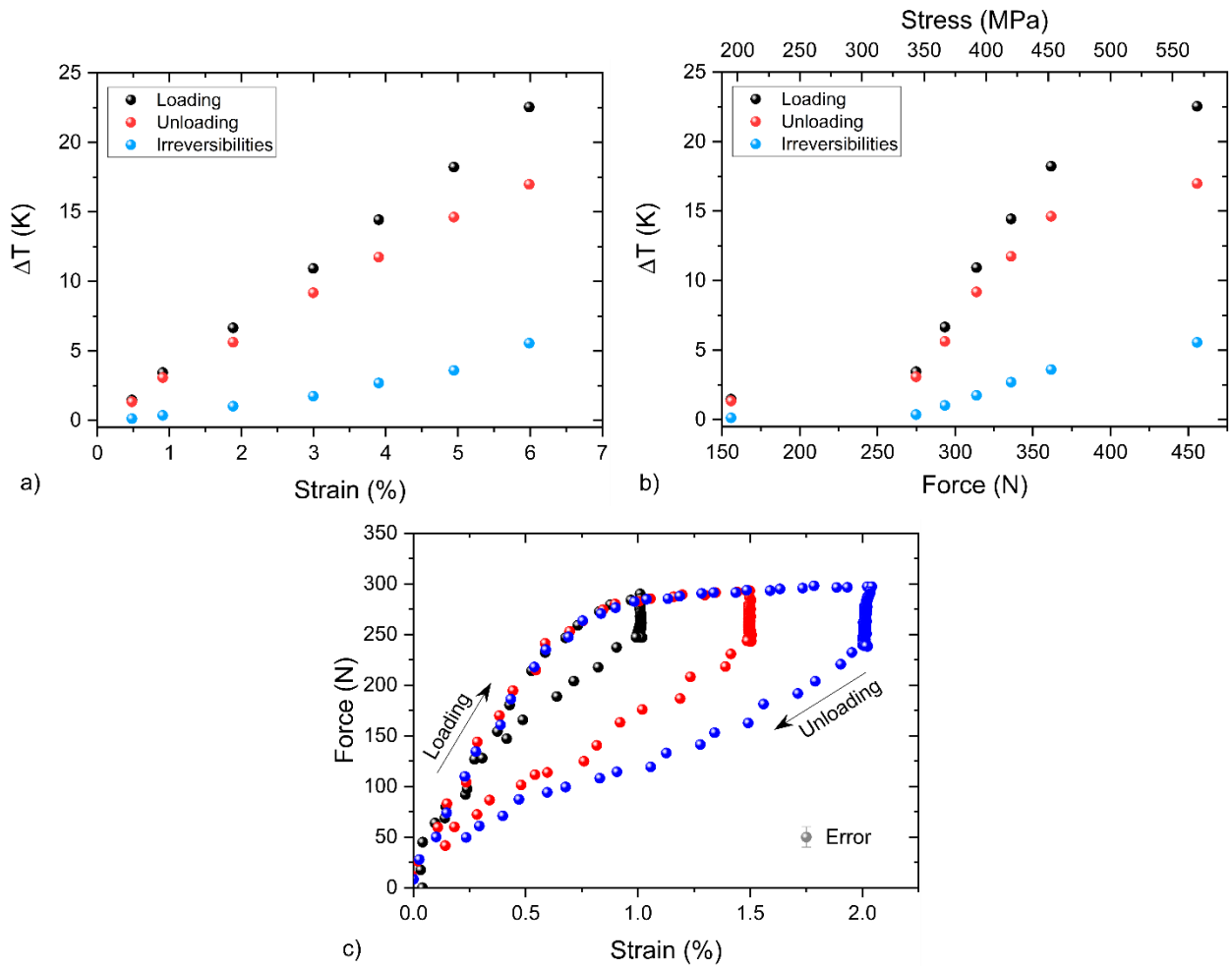

Figure 5 NiTi axially loaded. Temperature changes during axial loading and unloading as a function of (a) strain and (b) force. Errors in (a) and (b) are smaller than the size of the symbols. (c) Force-strain characteristics for 1, 1.5, and 2% strain with a representative error bar shown on the bottom right.

The temperature change increases with the strain in a near-linear fashion and the elastocaloric effect is higher for loading than unloading. At 6% strain, the measured temperature changes were 22.5 K and 17.0 K for loading and unloading, respectively. The difference in the temperature changes between loading and unloading results from elastocaloric material hysteresis and increases with rising strain. The temperature change is approximately linear with force from 1% to 5% strain. Below and above these values the increase in the force is much larger than rise in ΔT, indicative of the superelastic transformation from 1% to 5% strain. Below 1% the elastic deformation in the austenite is visible and above 5% the elastic

deformation in the martensite begins. The energy of hysteresis area amounts to 0.28, 1.65, and 2.89 MJ/m^3 for 1, 1.5, and 2% strain, respectively (Figure 5 (c)).

Trained NiTi strips were attached to the plastic beam of Figure 4 and tested in a four-point bending configuration. Results shown in Figure 6 were taken at the maximum possible strain rate that could be achieved at the maximum velocity (15 mm s^{-1}) of the actuator, i.e., 0.04 s^{-1}. This strain rate was slightly lower than the 0.05 s^{-1} possible during the axial loading due to longer travel distances required to achieve the same strain in four-point bending.

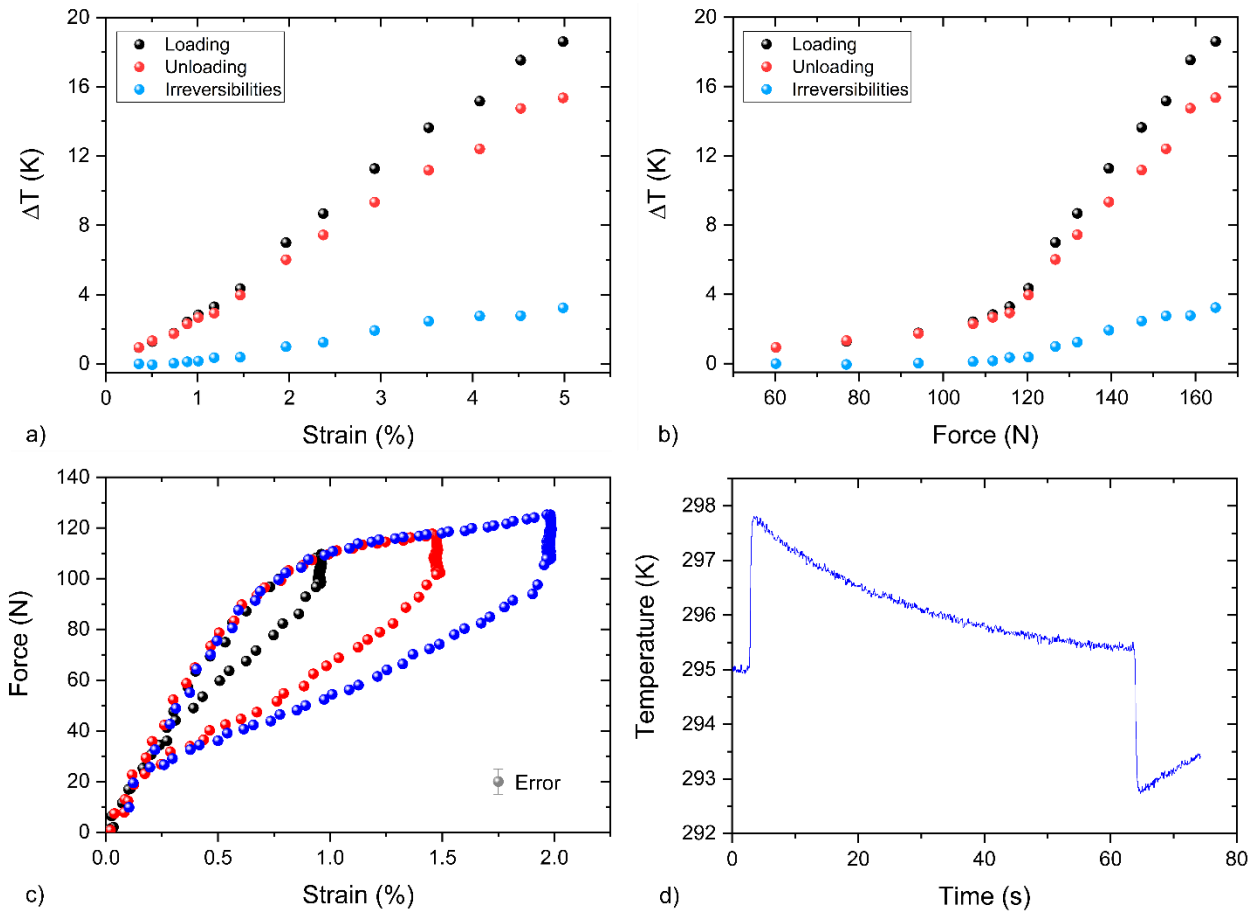

Figure 6 Composite beam subjected to bending with NiTi strip in tension. Temperature changes during loading and unloading as a function of (a) strain and (b) force. Errors in (a) and (b) are smaller than the size of the symbols. (c) Force-strain characteristics for 1, 1.5, and 2% strain with a representative error bar shown on the bottom right. (d) Typical record of temperature vs. time behavior of NiTi for 1% strain.

As seen in Figure 6 (a) and (b) the forces to reach a given strain are less than half of those required for the axially loaded sample. For the highest strain of 5% the temperature change was 18.6 and 15.4 K for loading and unloading, respectively. The ΔT values agree with results for axial loading at the same strain, even though slightly reduced strain rates may lead to slightly increased heat losses during the four-point bending.

With the present beam dimensions (see Figure 4), larger deflection results in thermal contact between the NiTi strip and the base material in the middle of the cutout.

With our new approach to elastocaloric actuation, the required force decreases at the expense of increased displacement. While low-force, high-displacement mechanism is a good match for the linear motor used in our experiments, this type of actuator may not be optimal for every application. The ability to tailor the required force and displacement profiles, on the other hand, opens up a wide design space that includes a variety of actuators and makes a large selection of variable-scale elastocaloric heat pump systems possible.

5 Bending, compressive loading

5.1 Samples

NiTi in tension suffers from fatigue at a low number of cycles which makes it desirable to operate the material in compression, however, thin strips of material buckle at very modest load for a given strip length. To overcome this limitation, we developed a composite beam consisting of a base beam material with a NiTi strip bonded to it (shown in Figure 7) allowing compressive stresses on the elastocaloric strip without buckling. Because the NiTi makes up a small portion of the beam, the neutral axis is in the base beam leaving the NiTi in pure compression with little variation over its thickness (approximately 8% according to COMSOL Multiphysics® finite element modeling, Supplementary figure 5). Using a four-point bend test configuration results in a large segment of the strip with constant compressive stress.

The PEEK beam used as a base material measured 150 mm long, 6.2 mm wide, and 6.2 mm thick. A NiTi strip was glued to the top surface of the beam using Loctite E-90FL epoxy. Before bonding, both surfaces were roughened with #80 grit abrasive paper and cleaned. The NiTi was also coated with AC-130-2 sol-gel to improve adhesion [21]. This configuration obscures one strip surface, limiting the heat transfer from the NiTi. Direct contact between the base beam and strips also results in heat transferred to the plastic (see below), reducing the measured temperature change of the NiTi compared to an unsupported strip in tension. This beam configuration allowed the 60 mm of NiTi between loading pins to be entirely in compression.

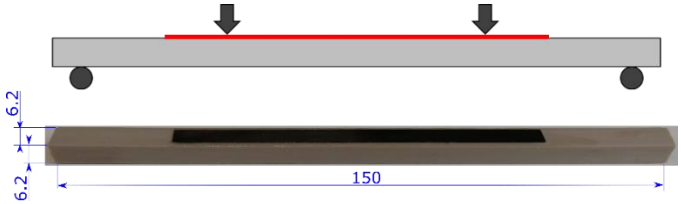

Figure 7 Sketch and photograph of the compression sample configuration with supporting pins shown by circles and loading pins shown by arrows

5.2 Results and discussion

The NiTi strips used in compressive mode were not trained due to the difficulty of applying direct compression at high strains and bonding issues between the NiTi and the PEEK. For strains above 1.5% samples typically failed at the joint after about 10 cycles on average, while at lower strains the bond withstands hundreds of cycles. After failure, the glue was routinely found to be entirely adhered to the NiTi with none remaining on the PEEK surface, suggesting that improving adhesion to PEEK (or using a different base material with high surface energy) could substantially lengthen sample life. Such an advancement is necessary before this method of actuating elastocaloric materials can be applied in cooling devices.

Results are presented in Figure 8. Similar to both axial and four-point bending tension, four-point bending compression experiments were performed at the maximum possible strain rate that could be achieved with the maximum velocity of the actuator. Considering geometries depicted in Figs. 4 and 7, the travel distance to achieve a given strain in compression is twice that for tension, which resulted in strain rate further reduced to 0.02 s^{-1}. Stress-strain characteristics for the composite beam for 1 and 1.5% strain show much lower hysteresis when compared with samples subjected to tension loading. No superelastic regime was observed, which agrees with results from [7,11], where superelasticity appeared for higher applied strains. The largest temperature change of 4.1 K for loading and unloading was obtained for 1.6% strain, with higher strains resulting in immediate glue joint failure. Temperature change was reversible which is consistent with a much narrower hysteresis compared to tension loading [7].

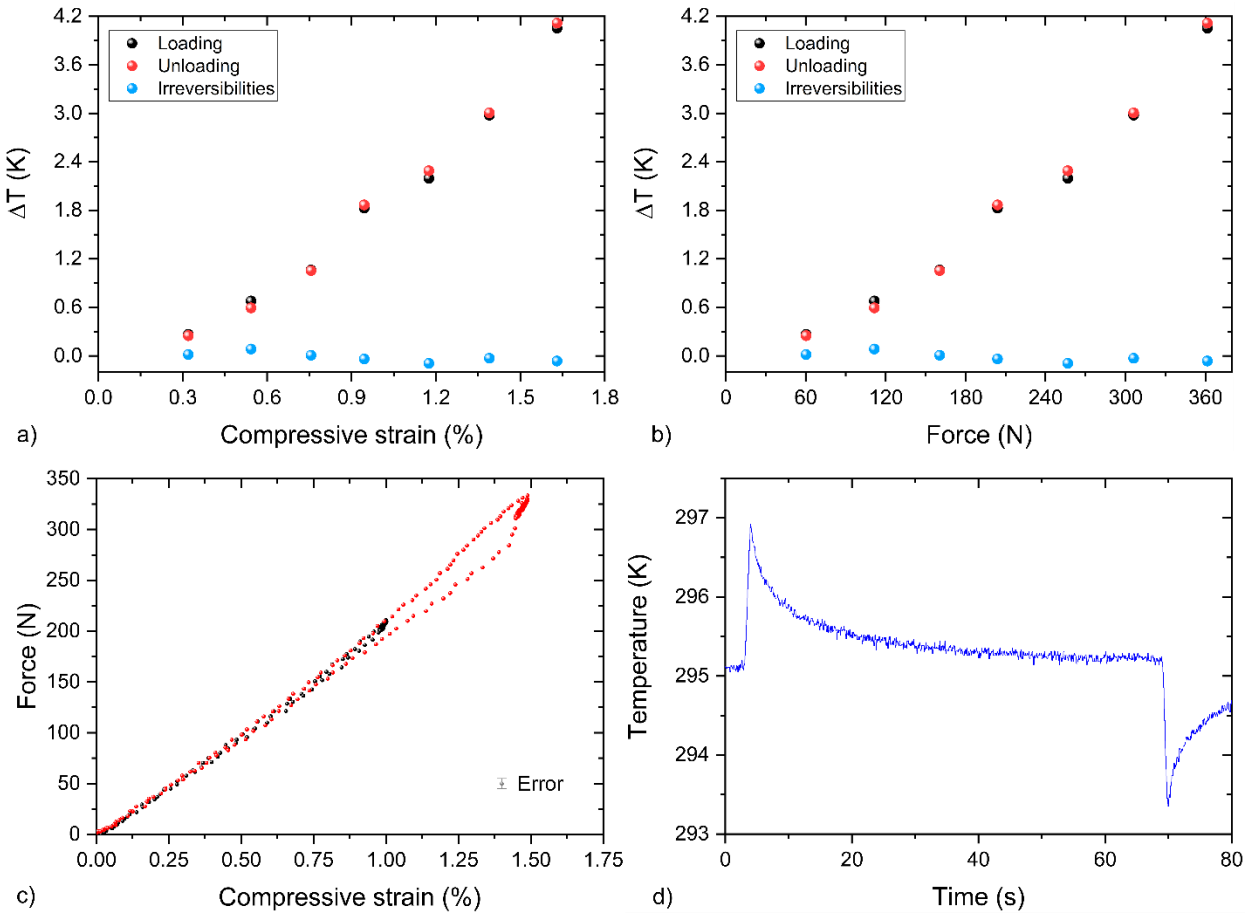

Figure 8 Composite beam subjected to bending with NiTi strip in compression. Temperature changes during loading and unloading as a function of (a) strain and (b) force. Errors in (a) and (b) are smaller than the size of the symbols. (c) Force-strain characteristics for 1 and 1.5% strain with a representative error bar shown on the bottom right. (d) Typical record of temperature vs. time behavior of NiTi for 1% strain.

Because of the sample dimensions, force cannot be applied axially to the sample without buckling to get a direct comparison between compression and bending. Results of the bending tests were used in conjunction with a COMSOL finite element model (Supplementary figure 5) to estimate Young's modulus of the NiTi and calculate the force required to directly compress the sample. The calculated value of 480 N for 1% strain is in agreement with published data [18]. The forces in bending are reduced by approximately half compared to the estimates for direct compression, and the risk of buckling of the NiTi strips is eliminated.

Selecting a low thermal conductivity material, such as PEEK, limits the amount of heat transferred to the beam, however, the direct contact does have an impact as revealed by the much faster return to room temperature compared to tensile-bending samples (Figure 8 (d)). The time to reduce the temperature by $\Delta T/2$ was 3.6 s for compression and 19.2 s for tension. Heat loss to PEEK can be esimated by comparing ΔT recorded in compression and tension. Assuming elastocaloric effects are the same in both cases [18], the difference in the two temperature changes under 1% strain gives the heat lost to the PEEK, Q_{lost},

$$Q_{lost} = Q_{tension} - Q_{compression} = \rho V c_p \left(\Delta T_{tension} - \Delta T_{compression}\right) \cong 0.22 \text{ J}, \quad (5)$$

were $Q_{tension}$ and $Q_{compression}$ – heats generated in tension and compression; ρ, V, c_p – density, volume, and specific heat of NiTi at constant pressure; $\Delta T_{tension}$ and $\Delta T_{compression}$ –temperature changes measured in tension and compression. To estimate the heat loss, ρ = 6500 kg m^{-3}, V = 48 mm^3, and c_p = 837 J kg^{-1} K^{-1} were used.

Heat transfer between PEEK and NiTi can also be estimated considering the response of a semi-infinite medium to a linear ramp in temperature following Carslaw and Jager [22], where heat flux into the PEEK is proportional to the square root of the product of the heat capacity, thermal conductivity, and density (also see Supplementary information). For the 1% strain shown in Figure 8, Q_{lost} is about 0.21 J, which is within 5% of that determined from Eq. 5. Heat losses to the beam can be reduced by selecting base material with lower specific heat, and/or density, and/or thermal conductivity. Faster actuation and reduced contact area between the active material and the base will further reduce heat losses. These options are currently under study and will be reported in the future.

Active regenerator(s) [23] based on the bending beam mechanism will require channels for oscillating fluid flow and larger quantities of the active (likely NiTi) material to demonstrate meaningful cooling power regardless of whether the actuation is performed in tension or compression. The amount of NiTi could be increased by either using a wider beam with a single NiTi sheet, or a regularly spaced stack of beams, each with a single NiTi strip, with flow channels arranged in thermal contact with the strips in both cases. More advanced designs may stack evenly spaced layers of NiTi attached to a single beam. Though the latter would result in strains varying from one layer to the next, the fluid flow(s) may then be realized between the layers.

6 Conclusions

Arranging elastocaloric strips in composite structures and subjecting the structures to actuating forces allows application of nearly-uniform, purely-tensile or purely-compressive stresses over large segments of the NiTi strips while greatly reducing the force required to achieve a given strain. A 50% lower force demand translates into smaller and simpler actuators. Another highly important feature of the proposed method is that thin strip samples can have high compression stresses applied without buckling, which is unreachable in direct loading. This result is very beneficial for construction of future elastocaloric systems, because the low fatigue life of materials subjected to tension limits their utility for practical devices. Strips also have much bigger surface to volume ratio compared to bulk materials which is important for efficient heat transfer. The proposed low-force and long-lifetime method of activating elastocaloric materials opens up new possibilities for construction of compact and efficient cooling and heating systems.

Data availability

The raw/processed data required to reproduce these findings cannot be shared at this time due to technical or time limitations. Data will be made available on request.

Acknowledgments

This work was performed under auspices of the caloric materials consortium, CaloriCool®, supported by the Advanced Manufacturing Office of the Office of Energy Efficiency & Renewable Energy and managed jointly through the Advanced Manufacturing and Building Technologies Offices of the U.S. Department of Energy. Ames Laboratory is operated for the U.S. Department of Energy by Iowa State University of Science and Technology under Contract No. DE-AC02-07CH11358.

References

[1] W. Goetzler, R. Zogg, J. Young, C. Johnson, Energy Savings Potential and RD&D Opportunities for Non-Vapor-Compression HVAC Technologies, 2014.

[2] A. Kitanovski, J. Tušek, U. Tomc, U. Plaznik, M. Ožbolt, A. Poredoš, Magnetocaloric Energy Conversion, 2015. doi:10.1007/978-3-319-08741-2.

[3] P. Weiss, A. Piccard, Le phénomène magnétocalorique, J. Phys. Theor. Appl. 7 (1917) 103–109.

[4] S. Jacobs, J. Auringer, A. Boeder, J. Chell, L. Komorowski, J. Leonard, S. Russek, C. Zimm, The performance of a large-scale rotary magnetic refrigerator, in: Int. J. Refrig., 2014. doi:10.1016/j.ijrefrig.2013.09.025.

[5] A. Greco, C. Aprea, A. Maiorino, C. Masselli, A review of the state of the art of solid-state caloric cooling processes at room-temperature before 2019, Int. J. Refrig. (2019). doi:10.1016/j.ijrefrig.2019.06.034.

[6] J. Tušek, K. Engelbrecht, D. Eriksen, S. Dall'Olio, J. Tušek, N. Pryds, A regenerative elastocaloric heat pump, Nat. Energy. (2016). doi:10.1038/nenergy.2016.134.

[7] J. Cui, Y. Wu, J. Muehlbauer, Y. Hwang, R. Radermacher, S. Fackler, M. Wuttig, I. Takeuchi, Demonstration of high efficiency elastocaloric cooling with large ΔT using NiTi wires, Appl. Phys. Lett. 101 (2012). doi:10.1063/1.4746257.

[8] S. Qian, Y. Geng, Y. Wang, J. Ling, Y. Hwang, R. Radermacher, I. Takeuchi, J. Cui, A review of elastocaloric cooling: Materials, cycles and system integrations, Int. J. Refrig. (2016). doi:10.1016/j.ijrefrig.2015.12.001.

[9] S. Qian, Y. Wu, J. Ling, J. Muehlbauer, Y. Hwang, I. Takeuchi, R. Radermacher, G.L.M. Hall, Design, developement and testing of a compressive thermoelastic cooling system, in: 24th IIR Int. Congr. Refrig., 2015. doi:10.18462/iir.icr.2015.0092.

[10] J. Tušek, A. Žerovnik, M. Čebron, M. Brojan, B. Žužek, K. Engelbrecht, A. Cadelli, Elastocaloric effect vs fatigue life: Exploring the durability limits of Ni-Ti plates under pre-strain conditions for elastocaloric cooling, Acta Mater. (2018). doi:10.1016/j.actamat.2018.03.032.

[11] K. Zhang, G. Kang, Q. Sun, High fatigue life and cooling efficiency of NiTi shape memory alloy under cyclic compression, Scr. Mater. (2019). doi:10.1016/j.scriptamat.2018.09.012.

[12] H. Hou, P. Finkel, M. Staruch, J. Cui, I. Takeuchi, Ultra-low-field magneto-elastocaloric cooling in a multiferroic composite device, Nat. Commun. (2018). doi:10.1038/s41467-018-06626-y.

[13] R. Wang, S. Fang, Y. Xiao, E. Gao, N. Jiang, Y. Li, L. Mou, Y. Shen, W. Zhao, S. Li, A.F. Fonseca, D.S. Galvão, M. Chen, W. He, K. Yu, H. Lu, X. Wang, D. Qian, A.E. Aliev, N. Li, C.S. Haines, Z. Liu, J. Mu, Z. Wang, S. Yin, M.D. Lima, B. An, X. Zhou, Z. Liu, R.H. Baughman, Torsional refrigeration by twisted, coiled, and supercoiled fibers, Science (80-.). 366 (2019) 216–

221. doi:10.1126/science.aax6182.
[14] D.J. Sharar, J. Radice, R. Warzoha, B. Hanrahan, B. Chang, First Demonstration of a Bending-Mode Elastocaloric Cooling "Loop," in: Proc. 17th Intersoc. Conf. Therm. Thermomechanical Phenom. Electron. Syst. ITherm 2018, 2018. doi:10.1109/ITHERM.2018.8419513.
[15] H. Ossmer, F. Wendler, M. Gueltig, F. Lambrecht, S. Miyazaki, M. Kohl, Energy-efficient miniature-scale heat pumping based on shape memory alloys, Smart Mater. Struct. (2016). doi:10.1088/0964-1726/25/8/085037.
[16] F. Bruederlin, H. Ossmer, F. Wendler, S. Miyazaki, M. Kohl, SMA foil-based elastocaloric cooling: From material behavior to device engineering, J. Phys. D. Appl. Phys. (2017). doi:10.1088/1361-6463/aa87a2.
[17] A. Kumar, A. Chauhan, S. Patel, N. Novak, R. Kumar, R. Vaish, Vibration induced refrigeration using ferroelectric materials, Sci. Rep. (2019). doi:10.1038/s41598-019-40159-8.
[18] Y. Wu, E. Ertekin, H. Sehitoglu, Elastocaloric cooling capacity of shape memory alloys – Role of deformation temperatures, mechanical cycling, stress hysteresis and inhomogeneity of transformation, Acta Mater. (2017). doi:10.1016/j.actamat.2017.06.012.
[19] F.P. Beer, R. Johnston, J. Dewolf, D. Mazurek, Mechanics of Materials, McGraw-Hill, New York. (1981).
[20] R. Prabhakaran, T.L. Galloway, Strain measurement in a shape memory alloy with strain gauges, Strain. (2005). doi:10.1111/j.1475-1305.2005.00228.x.
[21] T.J. Zimmerman, K.Y. Blohowiak, M.A. Dilligan, F.T. Calkins, J.H. Mabe, Adhesive bonding of hybrid actuated shape memory alloy-composite structures, in: SAMPE Fall Tech. Conf., 2010: pp. 1–13.
[22] H.S. Carslaw, J.C. Jaeger, Conduction of Heat in Solids, Oxford, Oxford Clarendon Press. 2nd. Ed. (1959). doi:10.1063/1.3057871.
[23] J.A. Barclay, W.A. Steyert, Active magnetic regenerator, (1982).